Investigation and optimization of polarization properties of self-assembled carbon nanotube films

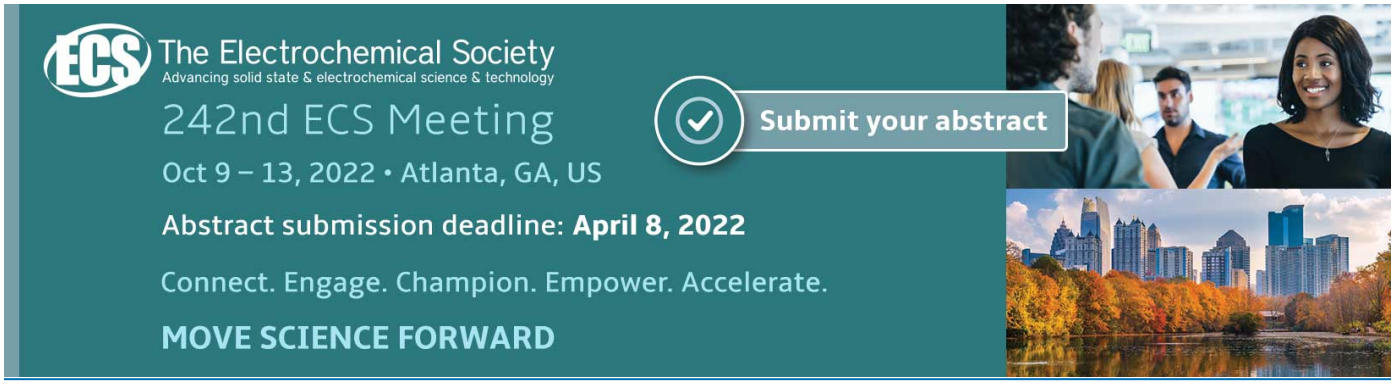

IOP Publishing Nanotechnology
Nanotechnology 33 (2022) 195702 (9pp) https://doi.org/10.1088/1361-6528/ac4d56

Investigation and optimization of polarization properties of self-assembled carbon nanotube films

Hui Zhang[1,2], Yibin Wang[1,2], Peng Zhang[1,2,*], Huwang Hou[2,3] and Yang Zhao[1,2,*]

[1] CAS Key Laboratory of Mechanical Behavior and Design of Materials, Department of Precision Machinery & Precision Instrumentation, University of Science and Technology of China, Hefei, Anhui 230027, People's Republic of China
[2] Key Laboratory of Precision Scientific Instrumentation of Anhui Higher Education Institutes, University of Science and Technology of China, Hefei, Anhui 230027, People's Republic of China
[3] Department of Modern Mechanics, University of Science and Technology of China, Hefei, Anhui 230026, People's Republic of China

E-mail: zhp9036@mail.ustc.edu.cn and yangz1@ustc.edu.cn

Received 16 November 2021, revised 13 January 2022
Accepted for publication 20 January 2022
Published 15 February 2022

Abstract

Super-aligned carbon nanotubes (CNTs) film has strong anisotropy to light propagation. In order to better integrate the self-assembled CNTs into microelectromechanical system (MEMS) for polarization applications, some inherent impacts on polarization properties of CNT film were investigated. We described the polarization effects of the film thickness variation in detail, giving an optimum thickness range which is around 700–800 nm. The amorphous carbon content of CNT film was reduced by oxidation process where the transmittance increased by almost 4 folds. The alignment of CNT arrangement was optimized from 0.41 (Chebyshev orientation parameter) to 0.54 by manipulating the C_2H_4 flow rate from 54 to 80 sccm. More specifically, a sample possessing a degree of polarization up to 99% and transmittance over 45% was obtained through proper regulations. The validated optimization makes the aligned CNT films more feasible and valuable for the integration of the CNT polarimeters with MEMS technology.

Keywords: carbon nanotube forest, water-assistant chemical vapor deposition, polarization control, CNT film thickness, nanotube alignment, growth defects of CNT

(Some figures may appear in colour only in the online journal)

1. Introduction

Polarization optics has various applications in polarization vision, biomedicine, and state control of electromagnetic waves [1–4]. The polarization vision above all can solve the great challenges of industrial vision inspection by harsh imaging environments such as low contrast and high reflectivity with typical devices including pixel-level polarizers and CMOS image sensing chips [5–8]. With the advancement in these chip-scale devices, the selection and property manipulation of an appropriate polarization material, which can be well compatible with the general MEMS fabrication process, become particularly urgent. Metal-grids are in common use for polarizers and polarization vision components for their high extinction ratios [9]. However, the ultrafine linewidth that requires an expensive and complicated electron beam photolithography process limits their large-scale production and applications [2, 10]. Multiple micro-polarizer arrays based on polymer thin films have been reported recently [11, 12], which hold a considerable extinction ratio and perform successfully in display applications. Even though, the excessive thickness of polymer material severely limits the light collection angle of the imaging element and increases the risk of pixel crosstalk [2, 13]. Therefore, seeking out a potential material that overcomes such inherent issues is needed.

* Authors to whom any correspondence should be addressed.

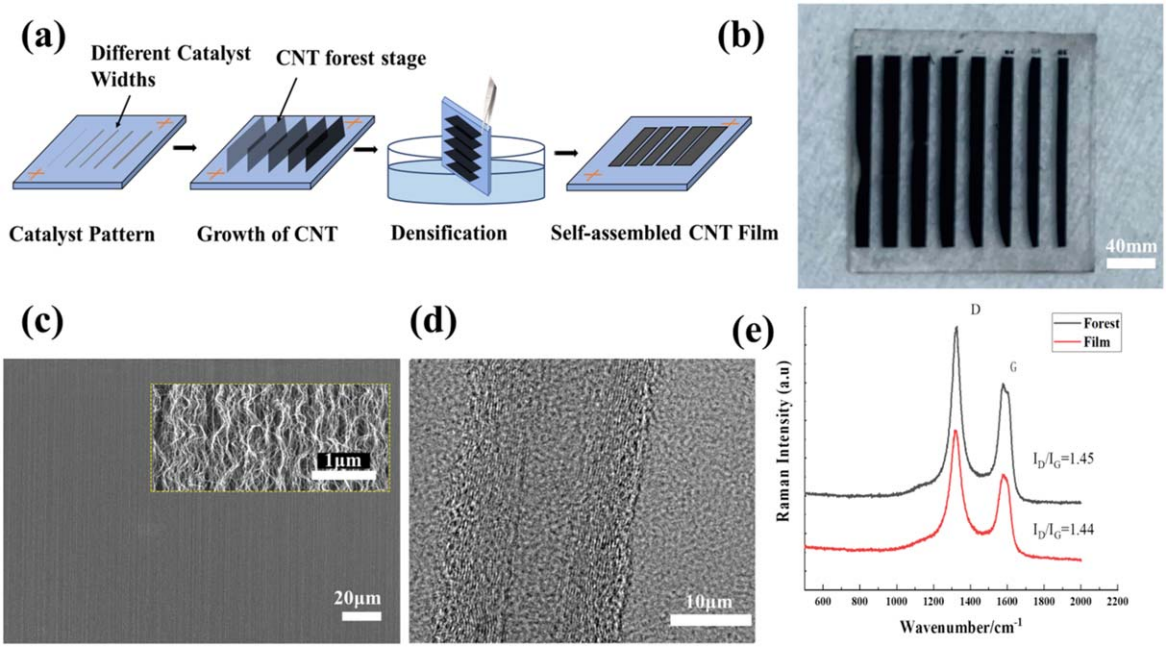

Figure 1. (a) Schematic illustration and fabrication process of self-assembled CNT film. (b) The self-assembled CNT films with different thickness on quartz. (c) The SEM images of densified self-assembled CNT film, scale bar 20 μm. Inset: enlarged SEM image, scale bar 1 μm. (d) The TEM image of single CNT, scale bar 10 nm. (e) The Raman spectra for CNTs forest and CNTs sheet.

Super-aligned carbon nanotubes, as a typical one-dimensional material, stand out as a promising candidate. Carbon nanotubes are typical anisotropic material and show apparent selectivity for light propagations [14]. When a light beam passes through a super-aligned CNT film, the photons with polarization perpendicular to the alignment direction of the CNTs pass through, whereas those parallel ones are absorbed [15]. Moreover, it can be synthesized by chemical vapor deposition (CVD) at a relatively low cost [16, 17], which could potentially reduce the production cost of polarizing devices significantly. Such unique property has easily aroused researchers' interest in exploring the specific polarization performance of CNTs. Extraordinary polarization capability was reported by Kaili Jiang *et al* [18] that aligned CNT yarns reached 92% degree of polarization (DOP) in the ultraviolet region at 325 nm wavelength. In the visible spectral range, the CNT film average transmittance of 60% and the DOP of 70% have been achieved simultaneously by moonyoung Jun *et al* [19]. Moreover, the extinction ratio(ER) of the CNT sheet polarizer reached ~37 dB in the broad terahertz range from 0.1 to 2.0 THz, which is regarded as a more prospective wave band [5]. Hence, not only does CNT own a relatively low cost, but also has attractive broadband anisotropic light-absorption properties. Taking the inherent flexibility and thermal stability into account [19–21], CNT films can be considered particularly promising in terms of integration into polarization image chips compared with traditional polymer films and metal-grid materials. However, to fit in these MEMS devices, CNT films should be well-controlled at properties and be placed at predefined locations with the required orientation direction of CNTs [22]. It is pretty challenging for the currently popular CNT film preparation method that is drawn from CNT forest into super-aligned yarns [23] when it comes to the precise transfer, adhesion, and integration into compact systems. On the other hand, the self-assembled CNT films can tackle such problems by growing the material on the appliance directly through prescribed configurations. Despite this, accurate control of self-assembled CNT film polarization properties still lacks sufficient support. Consequently, to reasonably regulate the polarization characteristics of self-assembled CNT film seems especially meaningful.

Herein, taking the self-assembled CNT films as research objects, three critical influencing factors on the polarizability of carbon nanotube films were discussed: the film thickness, the defects caused by imperfect growth environment, and the entanglements of tube bundles inside the film. We attempted to comprehend the mechanism of such effects and propose practically effective methods to regulate the polarization performances. Eventually, we successfully prepared pieces of self-assembled CNT films with DOP up to 99% and transmittance over 45% in the visible spectral region at 632 nm.

2. Experiment section

2.1. Preparation and characterization of self-assembled CNT film samples

The preparation process of self-assembled CNT film is schematically shown in figure 1(a). Here, alumina thin film (10 nm) was deposited on quartz wafer by atomic layer deposition (ALD), followed by the deposition of Fe film (2 nm) via thermal evaporation as catalyst layer [24, 25]. Photoresist lines with different widths varying from 30 to 100 μm were patterned on the catalyst by lithography, and the unexposed area was etched by inductively coupled plasma (ICP) to form a designed catalyst pattern. With a mixed gas

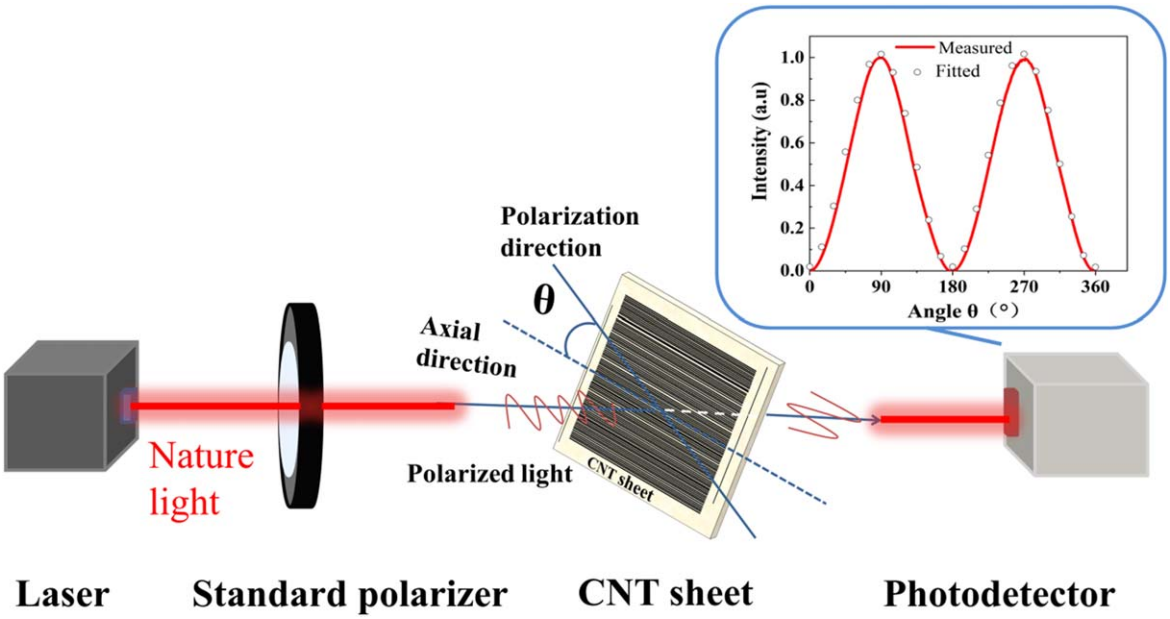

Figure 2. Schematic illustration of the CNT polarization detection method. And the correlation between light intensity received by photodetector and θ is displayed in diagram.

Table 1. Table shows the condition for synthesis of super-aligned CNT.

Type of CNTs	Substrate	Catalyst (nm)	Deposition technique	Gas (sccm)	Growth temperature (°C)	Growth time (min)	Height (mm)
MWCNTs	Quartz	Fe = 2	Thermal evaporation	Ar = 126 H_2 = 80 C_2H_4 = 54	760	30	1.5

flow of Ar (126 sccm), H_2 (80 sccm), H_2O (125 ppm), and C_2H_4 (54 sccm), the super-aligned CNT forests were grown at 680 °C over 30 min, and the maximum height of the forest reached 1.5 mm. The specific synthesis conditions are shown in table 1 [26, 27]. To obtain the densified film, the CNT forests were dipped into the 50% isopropanol solution. When the CNT forests are pulled out of the solution, the vertical CNT films fall laterally due to the surface tension at the gas–liquid interface. The sparse CNT forests become compact films because of the zippering effect of CNT bundles caused by liquid evaporation (figure 1(b)) [22].

The morphology of densified CNT film was inspected under the scanning electron microscope (SEM), demonstrating apparent alignment in figure 1(c). With the help of a transmission electron microscope (TEM), we found out that the CNTs are multi-walled with diameters close to 20 nm (figure 1(d)). The Raman spectra for CNTs forest and CNTs sheet were presented in figure 1(e). The integral ratio of peak D to peak G was used to estimate the structural changes before and after densification, showing no apparent differences.

2.2. Detection method of polarimetry on CNT film

Laser light with a wavelength of 632 nm was polarized by modulation of a standard polarizer (GCL-05, DHC, China) (figure 2). Diverse polarization states were acquired by rotating the standard polarizer with multiple angles. The orientation direction of CNTs was regarded as the axial direction of the CNT film sheet, and θ represents the angle between the axial direction and the polarization direction of the light. A photodetector was used behind the CNT sheet to receive the light intensity alterations corresponding to θ variations.

With θ rotated from 0° to 360° in 1° interval, the corresponding relationship between the light intensity passing through the CNT sheet and θ was achieved and shown in the inlet of figure 2. The curve shows that when the polarization direction of light is parallel to the axis of the CNT sheet ($\theta = 0°$), the transmittance is the minimum, while as the polarization direction of light is perpendicular to the axial direction ($\theta = 90°$), the transmittance is the maximum, which is in good agreement with that predicted by Malus's law, $I = I0\,\mathrm{COS}^2\alpha\left(\alpha = \frac{\pi}{2} - \theta\right)$, where I is the received light intensity, I_0 is the intensity of incident polarized light, and α is the angle between the polarized light and the polarization direction of the CNT sheet.

3. Results and discussion

3.1. Effect of CNT film thickness on polarization properties

The actual effective quantity of the CNT bundle determines the polarization performance of self-assembled CNT film in light modulation. When the particle density of the Fe catalyst is constant, the catalyst line width (see in figure 1(a)) plays a

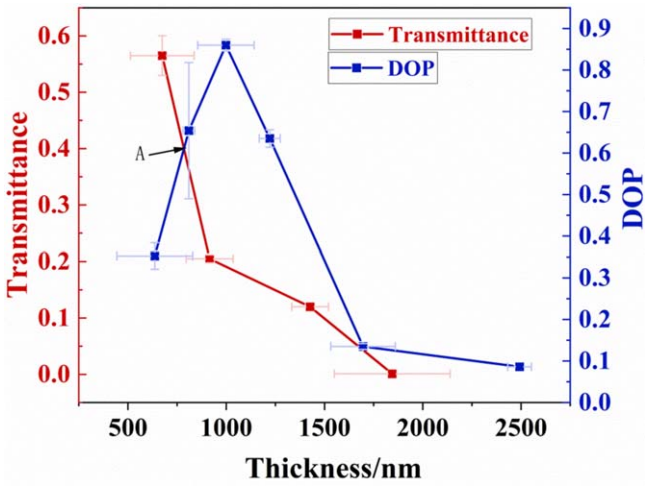

Figure 3. The corresponding DOP and transmittance variation curves with the increase of CNT thickness.

key part in the CNT quantity, which is represented as the different thicknesses among self-assembled CNT films. The density of CNT forest is ∼0.0138 g cm^{-3}, the height of CNT forest is ∼1 mm, and the weight percentage of catalyst in the CNT film is less than 0.11%. The wavelength of the light source is 632 nm where the absorption of Fe and Al_2O_3 are not sensitive [28, 29]. Hence, the negative impacts of catalyst on the polarization properties of the CNT film can be ignored. To explore the thickness influence on CNT properties, groups of CNT film samples containing multiple thickness alterations were prepared and measured by the step profiler (Bruker, Dektak XT), as shown in figure 1(b). The polarization property is usually characterized by the degree of polarization (DOP), expressing as:

$$\mathrm{DOP} = \frac{I\ \mathrm{max} - I\ \mathrm{min}}{I\ \mathrm{max} + I\ \mathrm{min}}, \tag{1}$$

where I_{max} and I_{min} denote the maximum and minimum light intensities received by a photodetector. The DOP ranges from 0 to 1, in which 0 means the device is totally unpolarized and 1 means an ideal polarizer. Film transmittance is also an essential characteristic for evaluating film performance in applications and is defined as the ratio of the maximum light intensity passing through the CNT sheet to the intensity of the incident light, $I_{max}/I_{incident}$. Therefore, DOP and transmittance were taken as two typical parameters to estimate the effect of film thickness on polarization capability (figure 3).

According to the Transmittance-thickness relationship (red line in figure 3), the transmittance generally shows a downward trend as the thickness increases. In the range of 500–1500 nm film thickness, the transmittance drops rapidly from over 59% to 12%, which indicates that a small variation in thickness will be accompanied by a rapid variation in transmittance. When the film thickness exceeds 1500 nm, the transmittance changes much more slowly with the variation of film thickness, and the film can be regarded as opaque. Mainly, the transmittance-thickness relationship can be regarded as monotonous, yet the circumstance is different in the DOP-thickness correlation as shown in figure 3 (blue line). The DOP shows an obvious upward trend in the thickness range of 500–1000 nm where the highest DOP can reach 90%, as the film thickness reaches around 1000 nm. Despite this, the DOP undergoes a precipitous decline after the film thickness exceeds 1000 nm and almost falls to 0 as it reaches 1500 nm and over, meaning the CNT film losses polarization capability completely.

The non-monotonic polarization phenomenon of CNT film can be related to the intrinsic microstructure of the film. Three stages of the CNT bundles accumulation process and a model of curved individual CNT (figure 4) were introduced to comprehend the internal mechanism. In the very first phase, thin CNT film contains a limited effective number of CNTs (figure 4(a)). Hence the transmittance is high while DOP is much lower as only a small proportion (parallel to the film axis) of light gets absorbed. With the reasonable accumulation of CNT bundles, the effective tube quantity per unit film surface becomes higher. In other words, the polarization capability of CNT film gets enhanced, represented by the increase of DOP. The transmittance always keeps a downward trend because of the strengthened absorption of light. Nevertheless, the rapid decrease of the DOP as the CNT film thickness exceeding a certain range indicates the loss of the alignment feature of the film. The SEM inspection (figure 1(c)) shows pretty good alignment among the CNT film. However, a closer look (inlet in figure 1(c)) indicates the wavey structure and entanglements between the tubes, which raises the loss of the polarization capability. Since individual CNT is curved, different parts exhibit dissimilar modulation of light. A coordinate (x–y) is defined along the general alignment direction of the CNT as illustrated in figure 4(b), with a sub-coordinate (x'–y') defines the direction of the curved CNT locally. The two coordinates make an intersection angle of β. When linearly polarized light passes through the specified section of the CNT, the polarimetric state of the light can be decomposed into two orthogonal components according to the local coordinate, and the component along the y'-axis will be absorbed. In the ideal case where the CNT is perfectly straight along the y-axis where $\beta = 0°$, light with polarization parallel to the x-axis will pass through completely. However, β varies along the tube due to the wavey nature of the CNTs, which means a small amount of the light polarized in the y'-axis exists and will be absorbed by the CNT. As a result, the CNT exhibits a certain absorptance of the horizontally polarized light. Once the number of CNTs gets excessive as the film becomes thicker, the absorption of the horizontal component (in the x-axis) becomes significant. In that case, the difference between I_{max} and I_{min} diminishes, which explains the rapid decline in DOP. Since transmittance and DOP are both crucial parameters in determining the polarization properties, the matching point A as an optimum point in figure 3 is marked out where the thickness is around 700–800 nm, transmittance close to 40%, and DOP over 60%.

3.2. Effect of growth defects on polarization properties

Following the root-growth [30, 31] discipline, the catalyst becomes less effective along the growing process, which

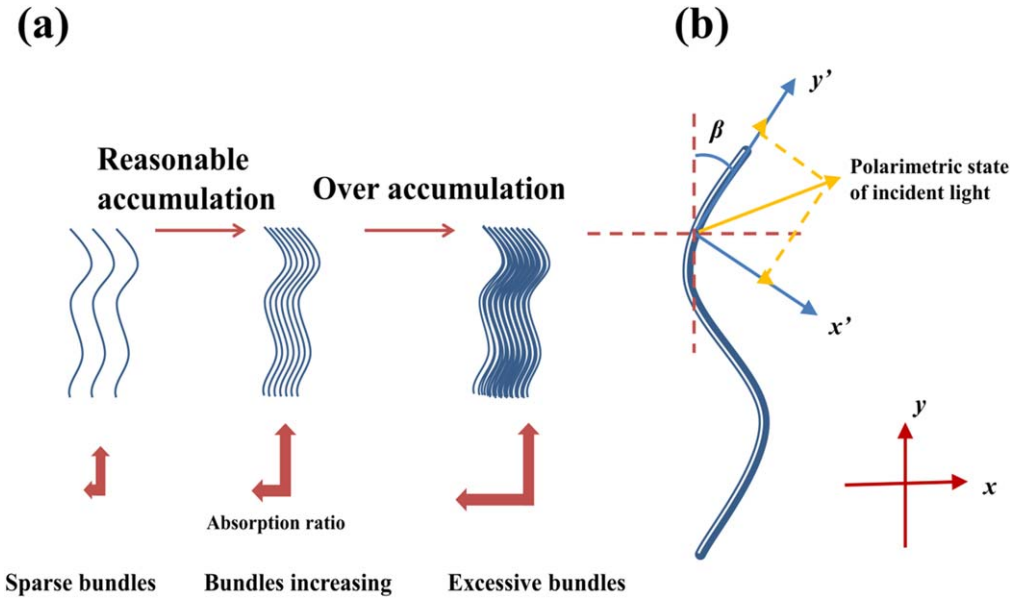

Figure 4. (a) Schematic illustration of CNT bundles accumulation process, accompanied by variations in absorption ratio of the horizontal and vertical components. (b) A curved CNT showing various modulations on polarization states at different location along the tube.

limits the height of the CNT forests. As a result, throughout the whole CNT film, especially the bottom part near the catalyst, possesses some defects inherently, such as amorphous carbon and incomplete single bundles. The morphology of the bottom CNT film under SEM is shown in figure 5(d) where the surface is covered with a layer of flocculent. This layer of flocculent is a mixture of amorphous carbon and defective CNTs. A mild post-growth oxidation process [21] was adapted to remove such a mixture. CNT films prepared on quartz substrate were etched with 100 ppm water vapor in argon at 400 °C for over 40 min After the mild oxidation process, the flocculent layer was effectively removed and the orientation arrangement of the CNT bundles became more obvious (figure 5(b)). The Raman spectra of CNT films before and after oxidation treatment was depicted in figure 5(c) where the integral ratio of peak D to peak G was used to estimate the content of amorphous carbon inside the CNT film. After water vapor etching, the ratio of I_D/I_G decreased from the original 1.78–1.47, indicating the decline of amorphous carbon content of CNT film [32, 33].

As demonstrated in figure 5(a), the polarization properties of the samples after the etching process are significantly improved. The transmittance of the sample is increased by almost 4 folds, and the DOP value increases from 0.17 to 0.33. This confirms that the amorphous carbon and outer edges of thick bundles were ablated [21] and the negative effect of them on polarization performance was alleviated with the post etching process.

3.3. Effect of CNTs alignment on polarization properties

The combination of thickness and defects controlling is still not adequate when the alignment of CNTs makes a critical impact on CNT optical performance. Many efforts have been made to explore the CNTs alignment effect on its optical and mechanical properties by methods of stretching [15], changing growth parameters [26, 27, 34], and immerging CNTs in solution with high magnetic fields [35, 36], etc. However, the investigation of the degree of alignment on the polarization capability of CNT film is still insufficient. As demonstrated above, the polarization performance of the CNT films are susceptible to film thickness, defects, etc. Therefore, a mechanical stretching method that changes the degree of alignment solely is adopted to eliminate the effects of other possible factors.

As depicted in figure 6(a), self-assembled CNT film was transferred to polydimethylsiloxane (PDMS) by direct printing [37]. The CNT film on the PDMS substrate was stretched with a translation stage along the alignment direction of the CNTs. Upon the stretching of the PDMS substrate, the deformation of the CNT film reaches about 9%, which is measured using optical method. Intensity-Angle curve was established in real time during the stretching process (figure 6(b)). Compared with the original CNT film, the maximum transmittance (I_{max}) of the stretched film is increased by 2.80%, while the minimum transmittance (I_{min}) decreased by 1.06%, leading to a 25.2% increase in DOP. Therefore, alignment of CNT bundles contributing an essential part in enhancing polarization capability of CNT film can be concluded.

3.4. Optimization of CNT film polarizer

It is pretty challenging to manipulate the polarization properties by stretching method when it comes to integration into MEMS devices with predefined locations and directions. Consequently, tunning of synthetic parameters can be regarded as a more practical method. Synthetic parameters concerned with CNT alignment can be categorized as catalyst density and chemical vapor percentages [34]. Considering the requirement of thickness control, the latter approach is more appropriate. Thus, the wafer with the same catalyst line width (~30 μm) corresponding

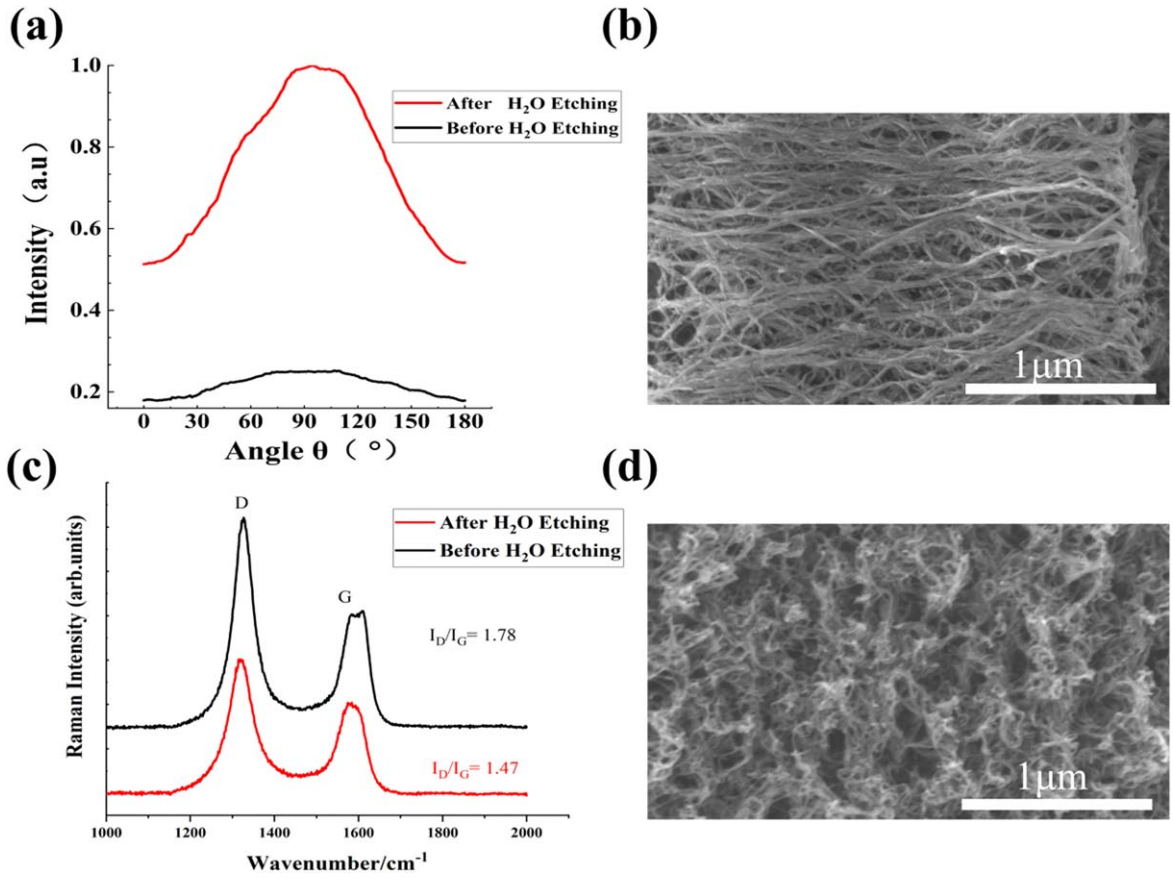

Figure 5. (a) Intensity-angle curves of the sample before and after H2O etching. (b) The CNT film after the water vapor etching process showing clean CNT bundles with good alignments; (c) the Raman spectra of CNT film before and after oxidation treatment of water vapor. The ratio of I_D/I_G decreased after oxidation process indicates the decline of amorphous carbon content inside the CNT film. (d) The as-grown CNT film showing excessive amorphous carbon.

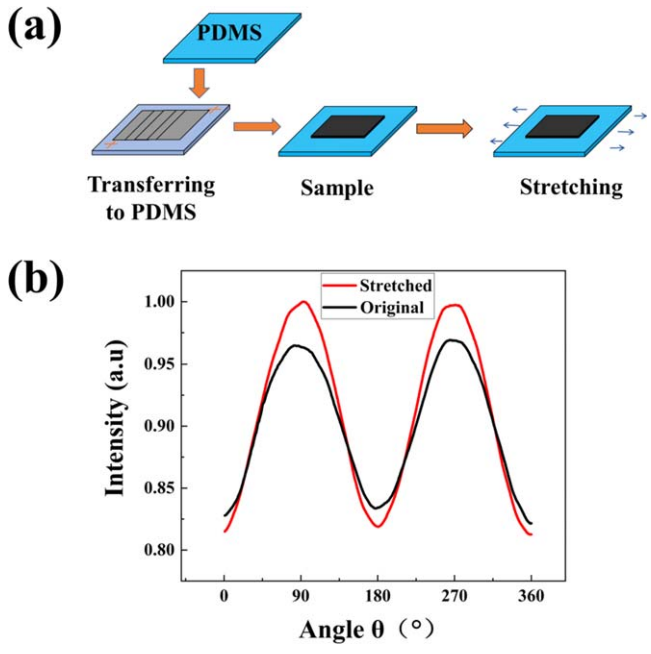

Figure 6. (a) Schematic process of CNT film transferring and stretching. (b) The intensity-angle curves of original and stretched CNT film.

to the matching point in figure 3 was grown in different circumstances. Figure 7 (a) shows the SEM of the CNT film sample grown under the original circumstance. With the C_2H_4 flow rate increased from 54 to 80 sccm, CNT samples with better alignment were synthesized (figure 7(b)).

To quantitatively evaluate the alignment of the samples, 2D fast Fourier transfer (FFT) was applied to figure (a) and (b) to illustrate the structures in the spectrum domain. Based on the spectrums of the images, Chebyshev orientation parameter (COP) [38, 39] for planar (2D) surface was introduced to calculate the orientation degree as:

$$\mathrm{cop} = 2\langle \cos^2 \varphi \rangle 2\mathrm{D} - 1 \tag{2}$$

$$\langle \cos^2 \varphi \rangle 2\mathrm{D} = \frac{\int_0^{\pi} I(\varphi)\cos_{\varphi}^2 d\varphi}{\int_0^{\pi} I(\varphi) d\varphi}, \tag{3}$$

where φ is the angle between the structural unit vector and the reference direction range from 0 to π, as shown in figure 7(d). $I(\varphi)$ represents the intensity distribution function (IDF) (figures 7(e) and (f)), as a function of φ from 0 to π, which represents the azimuthal scans summed over a range of radius according to the spectral distribution in FFT images. Under

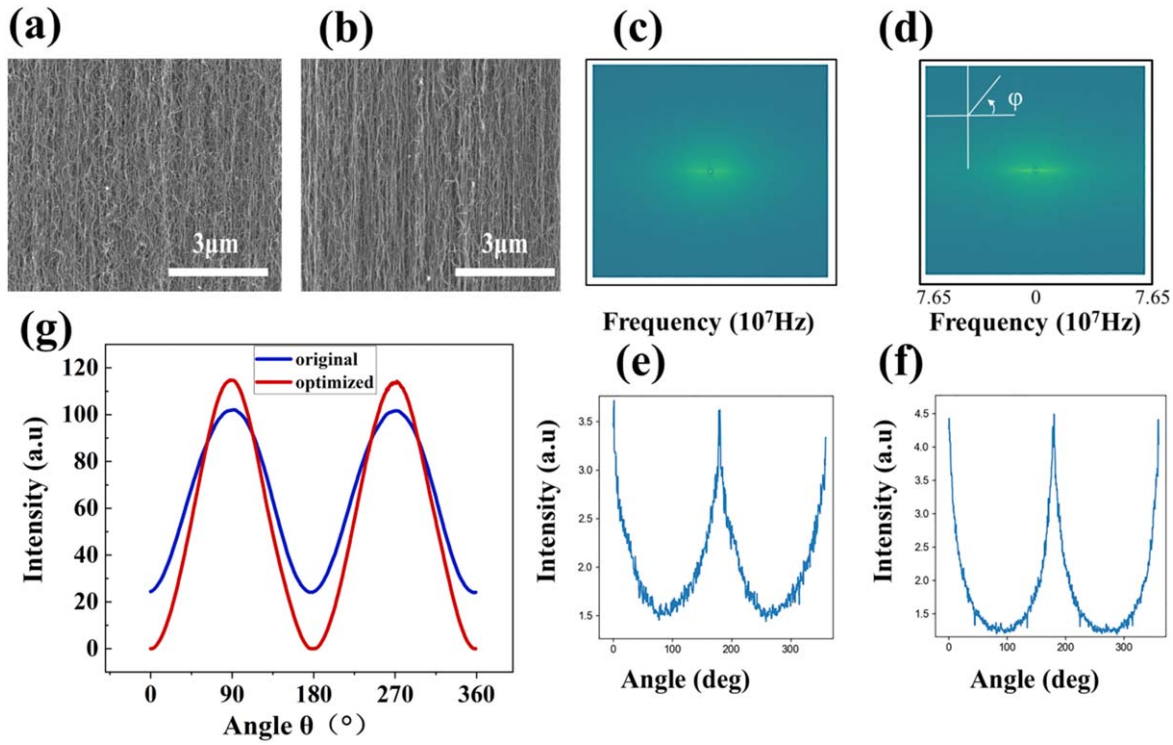

Figure 7. (a) The SEM image of CNT film with original growing parameters with 54 sccm flow rate of C_2H_4. (b) The SEM image of CNT film with synthetic parameters optimized (80 sccm flow rate of C_2H_4). (c) And (d) are the FFT images of SEM image (a) and (b), respectively. (e) and (f) are the intensity distribution functions (IDFs) derived from FFT image (c) and (d) respectively, showing a peak at 180°. (g) The intensity-angle curves of original and optimized CNT film, respectively.

the same quantified standards, the COP of two samples was calculated and figure (a) and (b) yield COP of 0.41 and 0.54, respectively. The increase in COP from sample (a) to sample (b) indicates that the alignment was improved by varying growing circumstances. With the improvement of the alignment and the optimized film thickness, a DOP close of 99% was achieved (figure 7(g)). Moreover, thanking the post H_2O etching, the transmittance increased to 45% simultaneously.

4. Conclusion

Due to the applicability in a wide electromagnetic band of anisotropy and low cost synthesis process, exploring the mechanism and proposing proper methods of improving its polarization capability makes a significant advance in the integration of CNT film polarizers into MEMS devices. Based on the growth characteristics and morphology of CNTs, the thickness of the film, growing defects, and the alignment of CNT bundles were considered as three main effects on the degree of polarization of CNT films. Mechanisms of the above factors on polarization properties of CNT films were explored in detail, aiming at the perspective of their integration with MEMS devices. As can be concluded from the investigations, the film thickness is the most vital factor in determining the polarization capability of CNT film. While the thickness keeps constant, alignment control plays a critical part in regulating the polarization performance, which can be adjusted with growth parameters in practice. Amorphous carbon mainly influents the transmittance. Combining the thickness control, the impurity removal, and the improvement in alignment in CNT films mentioned above, a CNT film polarizer possessing a DOP close to 99% and transmittance over 45% was obtained.

Acknowledgments

This work was supported by the National Natural Science Foundation of China (#11772321& #51732006)The authors would like to thank USTC Center for Micro- and Nanoscale Research and Fabrication and Experimental Center of Engineering and Material Science of USTC for their supports in sample fabrication and analysis. The authors are thankful for Prof. Qingwen Li, Prof. Jiangtao Di, and their research group in Suzhou Institute of Nano-Tech and Nano-Bionics (SINANO), Chinese Academy of Sciences, for the consultants in CNT synthesis.

Data availability statement

The data generated and/or analysed during the current study are not publicly available for legal/ethical reasons but are available from the corresponding author on reasonable request.

Funding

National Natural Science Foundation of China (#11772321& #51732006).

Disclosures

The authors declare no conflicts of interest.

ORCID iDs

Yang Zhao https://orcid.org/0000-0002-3962-2793

References

[1] Xu Q, Chen L, Wood M G, Sun P and Reano R M 2014 Electrically tunable optical polarization rotation on a silicon chip using Berry's phase *Nat. Commun.* **5** 5337
[2] Guo B and Brady D 2000 Fabrication of thin-film micropolarizer arrays for visible imaging polarimetry *Appl. Opt.* **39** 1486–92
[3] Rubin N A, D'Aversa G, Chevalier P, Shi Z and Capasso F 2019 Matrix Fourier optics enables a compact full-Stokes polarization camera *Science* **365** eaax1839
[4] Kuncic Z, McNamara A, Wu K and Boardman D 2011 Polarization enhanced x-ray imaging for biomedicine *Nucl. Instrum. Methods Phys. Res. A* **648** S208–10
[5] Kyoung J, Jang E Y, Lima M D, Park H R, Robles R O, Lepro X, Kim Y H, Baughman R H and Kim D S 2011 A reel-wound carbon nanotube polarizer for terahertz frequencies *Nano Lett.* **11** 4227–31
[6] Wu D, Guo J, Du J, Xia C, Zeng L, Tian Y, Shi Z, Tian Y, Li X J and Tsang Y H 2019 Highly polarization-sensitive, broadband, self-powered photodetector based on graphene/PdSe2/germanium heterojunction *ACS nano* **13** 9907–17
[7] Wu Y *et al* 2014 Hybrid graphene-microfiber waveguide for chemical gas sensing *IEEE J. Selected Topics Quantum Electronics A Publication IEEE Lasers & Electro Opt. Soc.* **20** 49–54
[8] Yang L, Hu T, Hao R, Qiu C, Xu C, Yu H, Xu Y, Jiang X, Li Y and Yang J 2013 Low-chirp high-extinction-ratio modulator based on graphene–silicon waveguide *Opt. Lett.* **38** 2512–5
[9] Zhang Z, Dong F, Cheng T, Qiu K, Zhang Q, Chu W and Wu X 2014 Nano-fabricated pixelated micropolarizer array for visible imaging polarimetry *Rev. Sci. Instrum.* **85** 105002
[10] Hsu W-L, Balakrishnan K, Ibn-Elhaj M and Pau S 2014 Infrared liquid crystal polymer micropolarizer *Appl. Opt.* **53** 5252–8
[11] Guo J and Brady D J 1997 Fabrication of high-resolution micropolarizer arrays *Opt. Eng.* **36** 2268–71
[12] Hamamoto T, Toyota H and Kikuta H 2001 Microretarder array for imaging polarimetry in the visible wavelength region *Int. Soc. Opt. Photonics* **440** 293–300
[13] Gruev V, Ortu A, Lazarus N, Van der Spiegel J and Engheta N 2007 Fabrication of a dual-tier thin film micropolarization array *Opt. Express* **15** 4994–5007
[14] DeHeer W A, Bacsa W, Chatelain A, Gerfin T, Humphrey-Baker R, Forro L and Ugarte D 1995 Aligned carbon nanotube films: production and optical and electronic properties *Science* **268** 845–7
[15] Fagan J A, Simpson J R, Landi B J, Richter L J, Mandelbaum I, Bajpai V, Ho D L, Raffaelle R, Walker A and Bauer B J 2007 Dielectric response of aligned semiconducting single-wall nanotubes *Phys. Rev. Lett.* **98** 147402
[16] Hata K, Futaba D N, Mizuno K, Namai T, Yumura M and Iijima S 2005 Water-assisted highly efficient synthesis of impurity-free single-walled carbon nanotubes *Abstracts Papers Am. Chem. Soc.* **229** U967-U
[17] Murakami Y, Chiashi S, Miyauchi Y, Hu M, Ogura M, Okubo T and Maruyama S 2004 Growth of vertically aligned single-walled carbon nanotube films on quartz substrates and their optical anisotropy *Chem. Phys. Lett.* **385** 298–303
[18] Jiang K L, Li Q Q and Fan S S 2002 Nanotechnology: spinning continuous carbon nanotube yarns - carbon nanotubes weave their way into a range of imaginative macroscopic applications *Nature* **419** 801
[19] Jung M, Noh Y, Suh D and Ahn S E 2018 Flexible and thermally stable optical polarizers based on highly aligned carbon nanotube sheets for the visible spectral range *Adv. Mater. Technol.* **3** 1800203
[20] Peng L M, Zhang Z L, Xue Z Q, Wu Q D, Gu Z N and Pettifor D G 2000 Stability of carbon nanotubes: how small can they be? *Phys. Rev. Lett.* **85** 3249–52
[21] Feng C, Liu K, Wu J S, Liu L, Cheng J S, Zhang Y, Sun Y, Li Q, Fan S and Jiang K 2010 Flexible, stretchable, transparent conducting films made from superaligned carbon nanotubes *Adv. Funct. Mater.* **20** 885–91
[22] Hayamizu Y, Yamada T, Mizuno K, Davis R C, Futaba D N, Yumura M and Hata K 2008 Integrated three-dimensional microelectromechanical devices from processable carbon nanotube wafers *Nat. Nanotechnol.* **3** 289–94
[23] Wei Y, Lin X Y, Jiang K L, Liu P, Li Q Q and Fan S S 2013 Thermoacoustic chips with carbon nanotube thin yarn arrays *Nano Lett.* **13** 4795–801
[24] Im J *et al* 2009 Direct printing of aligned carbon nanotube patterns for high-performance thin film devices *Appl. Phys. Lett.* **94** 053109
[25] Zhang P, Guo J, Hou H, Zhang Y, Yang X, Zhong H, Chen L and Zhao Y 2020 Highly aligned carbon nanotube-based bi-material microactuators with reduced intertube slipping *ChemNanoMat* **6** 404–11
[26] Sharma P, Pavelyev V, Kumar S, Mishra P, Islam S and Tripathi N 2020 Analysis on the synthesis of vertically aligned carbon nanotubes: growth mechanism and techniques *J. Mater. Sci., Mater. Electron.* **31** 4399–443
[27] Hahm M G, Hashim D P, Vajtai R and Ajayan P M 2011 A review: controlled synthesis of vertically aligned carbon nanotubes *Carbon Lett.* **12** 185–93
[28] Lynch D W and Hunter W 1997 *Handbook of Optical Constants of Solids* (Amsterdam: Elsevier) pp 341–419
[29] Gervais F 1998 *Handbook of Optical Constants of Solids* (Amsterdam: Elsevier) pp 761–75
[30] Baker R 1989 Catalytic growth of carbon filaments *Carbon* **27** 315–23
[31] Gavillet J, Loiseau A, Journet C, Willaime F, Ducastelle F and Charlier J-C 2001 Root-growth mechanism for single-wall carbon nanotubes *Phys. Rev. Lett.* **87** 275504
[32] Osswald S, Havel M and Gogotsi Y 2007 Monitoring oxidation of multiwalled carbon nanotubes by Raman spectroscopy *J. Raman Spectros.* **38** 728–36
[33] Behler K, Osswald S, Ye H, Dimovski S and Gogotsi Y 2006 Effect of thermal treatment on the structure of multi-walled carbon nanotubes *J. Nanopart. Res.* **8** 615–25
[34] Xu M, Futaba D N, Yumura M and Hata K 2012 Alignment control of carbon nanotube forest from random to nearly perfectly aligned by utilizing the crowding effect *ACS Nano* **6** 5837–44

[35] Shaver J, Crooker S, Fagan J, Hobbie E, Ubrig N, Portugall O, Perebeinos V, Avouris P and Kono J 2008 Magneto-optical spectroscopy of highly aligned carbon nanotubes: Identifying the role of threading magnetic flux *Phys. Rev. B* **78** 081402

[36] Shaver J, Parra-Vasquez A N G, Hansel S, Portugall O, Mielke C H, Von Ortenberg M, Hauge R H, Pasquali M and Kono J 2009 Alignment dynamics of single-walled carbon nanotubes in pulsed ultrahigh magnetic fields *ACS Nano* **3** 131–8

[37] Im J, Lee I-H, Lee B Y, Kim B, Park J, Yu W, Kim U J, Lee Y H, Seong M-J and Lee E H 2009 Direct printing of aligned carbon nanotube patterns for high-performance thin film devices *Appl. Phys. Lett.* **94** 053109

[38] Kaniyoor A, Gspann T S, Mizen J E and Elliott J A 2021 Quantifying alignment in carbon nanotube yarns and similar two-dimensional anisotropic systems *J. Appl. Polym. Sci.* **138** 50939

[39] Klug H P and Alexander L E 1974 X-ray diffraction procedures: for polycrystalline and amorphous materials (p 992)